Heliyon 11 (2025) e41736

Contents lists available at ScienceDirect

Heliyon

journal homepage: www.cell.com/heliyon

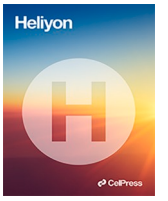

Research article

Identification and analysis of prognostic ion homeostasis characteristics in kidney renal clear cell carcinoma

Xiangmin Zhang [1], Xiongxian Qian [1], Yong Zhao, Maofei Ye, Liyang Li, Jian Chu [*]

Department of Urology, Shanghai Baoshan Luodian Hospital, Baoshan District, Shanghai, 201908, China

ARTICLE INFO

Keywords:
Oncology
Kidney renal clear cell carcinoma
Bioinformatics
Signature

ABSTRACT

Kidney renal clear cell carcinoma (KIRC), a prevalent primary malignant tumor within the urinary system, is characterized by significant heterogeneity. It has been shown that ion channels are important targets for anti-tumor therapy. In this study, we screened 70 selected KIRC related ion homeostasis genes with significant differential expression. We established diagnostic and prognostic models for 15 genes (PDK4, JPH4, ATP1A3, CCL7, CYP27B1, ABCB6, TNFSF11, MCHR1, TNNI3, ANGPTL3, Ednrb, SAA1, Chrna9, TMPRSS6, CCL14) by LASSO regression in the TCGA-KIRC cohort. We also provided a nomogram based on ion homeostasis for clinicians to explore the combined effect of the risk model on clinical variables. Patients in the low-risk group have a significant survival advantage. The potential clinical benefit of our predicted 15 gene signatures in clinical strategies was validated by Calibration Curves and DCA curves. Ultimately, the immune microenvironment and enrichment pathways were analyzed among individuals categorized as high-risk and low-risk. The predictable ion homeostasis-associated 15 gene signature established in this study predicts overall survival outcomes in patients with KIRC, to some extent helping clinicians to select personalized treatment regimens.

1. Introduction

According to histological and molecular subtypes, clear cell carcinoma is the most prevalent type of renal cell carcinoma [1], which is the primary form of urogenital cancer with a mortality rate of 30–40 % [2]. At present, the treatment strategy of renal clear cell carcinoma is limited [3]. In cancers, genes encoding ion channels are present [4]. Membrane proteins responsible for intracellular and intercellular signaling, membrane proteins used to couple extracellular events to intracellular reactions and to maintain intracellular ion homeostasis channels contribute [1,4], to varying degrees, to the Pathophysiology characteristics of each cancer signature. Studies have shown that cancer markers and ion channel dysfunction are causally related to genetic mutations in ion channel genes that alter the biophysical properties of the channels because of disease states [5,6]. As a result, there is an urgent necessity for additional innovative biomarkers to forecast the outlook of individuals suffering from early-stage KIRC. This will enable timely execution of clinical interventions to prolong disease advancement. Different ion channels regulate the immune system's recognition and elimination of tumor cells, playing a unique role [7,8]. Ion channels exhibit distinct behavior in tumor cells compared to immune cells, resulting in increased polarization and impacting the proliferation and spread of tumor cells. We performed a lasso regression on ion homeostasis-related genes with significant expression differences in KIRC ($|\log FC| > 2$, $P < 0.05$) to screen for prognostic genes among

* Corresponding author.
E-mail address: doctor_chu@126.com (J. Chu).
[1] These authors contributed equally: Xiangmin Zhang and Xiongxian Qian.

https://doi.org/10.1016/j.heliyon.2025.e41736
Received 15 July 2024; Received in revised form 4 January 2025; Accepted 5 January 2025
Available online 6 January 2025

them, establishing a risk model. The differential expression of prognostic genes was analyzed. For each patient, riskScore (RS) was measured using the formula. Based on the median risk coefficient, we divided patients into high-risk and low-risk categories. We utilized the Kaplan-Meier method to generate ROC curves for survival predictions at 1-year, 3-year, and 5-year intervals. In parallel, the infiltration levels of 23 distinct immune cell types within the KIRC immune microenvironment were analyzed using a deconvolution algorithm that applied the risk coefficient. The correlation analysis showed that the prognostic gene model may affect the tumor microenvironment as well, and may affect the prognosis of KIRC through direct or indirect molecular mechanism.

2. Materials and methods

2.1. Materials and methods data collection

Data on mRNA sequencing in cancer patients with clear cell renal cell carcinoma (KIRC) were gathered from the TCGA database. The dataset consisted of 613 samples, comprising 72 adjacent normal tissues and 541 tumor tissues. A subset of 537 individuals with available clinical details were chosen for analysis, excluding those lacking corresponding RNA sequencing data. The expression levels of genes were measured in terms of "fragments per kilobase million", which were then transformed into "millionths of transcripts" for further analysis. The external dataset (E-MTAB-1980) was obtained from the ArrayExpress database and contains information on 101 KIRC samples.

2.2. Acquisition of DEion homeostasis-related genes

A total of 524 genes associated with "Ion homeostasis" were downloaded from the Harmony portal(https://maayanlab.cloud/Harmonizome/gene_set/ion+homeostasis/GO+Biological+Process+Annotations). In addition, genes related to "ion homeostasis" were extracted from the TCGA-KIRC queue, and 70 DEGs related to ion homeostasis were identified using the "Limma" R package, with a threshold of $|\log FC|>2$ and $p < 0.05$ [9].

2.3. Enrichment analysis

Software packages were used to conduct Gene Ontology (GO) [10] and Kyoto Encyclopedia of Genes and Genomes (KEGG) analyses, following an accepted threshold [11].

To enhance significance, p-values underwent FDR adjustment. Utilizing the "GSVA" package in R-software, Gene Set Variation Analysis (GSVA) was executed. Employing a non-parametric unsupervised method, the analysis converted a conventional gene matrix into a sample-by-sample gene set, yielding an enrichment score for every sample and pathway [12].

2.4. Machine learning selection of biomarkers

In order to build a predictive model with exceptional performance, machine learning models were employed to identify genes that are strongly linked to prognosis. Gene expression levels were standardized using the "Log2+1″ and "Minmax" normalization techniques. Using LASSO algorithm, perform dimensionality reduction and feature selection analysis on central genes related to prognostic outcomes to avoid overfitting and deletion of closely related genes. Use 10 fold cross validation to select the minimum penalty term (λ). The coefficients obtained from LASSO regression were used to calculate a risk score equation for each standardized gene expression level [13].

$$\text{risk}Score = \sum_i Coefficient\ (hub\ gene_i) * mRNA\ Expression\ (hub\ gene_i) \quad ①$$

2.5. The construction and validation of risk model

The significant gene values were computed in both models, and the top 11 genes were identified as key genes for subsequent investigation. Analysis of survival indicated variance in overall survival. Furthermore, Analysis of Cox regression was performed to determine independent predictors of prognosis. Discrimination and calibration were assessed using ROC and calibration curves, respectively [14].

2.6. Construction and evaluation of a predictive nomogram

A nomogram was formulated based on clinicopathological features and risk assessments. To confirm its accuracy, an internal validation was performed using a calibration plot. The predictive performance of the nomogram was evaluated by employing the Time-C index. Moreover, the clinical net benefit was analyzed via Decision Curve Analysis (DCA).

2.6.1. Evaluation of tumor microenvironment (TME)

Implement the CIBERSORT algorithm using the R programming language to evaluate the TME condition in each sample collected from patients with KIRC. The CIBERSORT tool was utilized to estimate the proportions of 22 different TILs within the KIRC samples. To

Table 1
Target sequences.

Gene	Target sequences (5′-3′)
si-EDNRB_1	CTGAAACTTGGCTCTGAAACTGC
si-EDNRB_2	TCGAGATCAAGGAGACTTTCAAA

Table 2
The primer pair sequences of the studied genes.

Gene	Forward primer sequence (5′-3′)	Reverse primer sequence (5′-3′)
CCL4	GCTTCCTCGCAACTTTGTGGTAG	GGTCATACACGTACTCCTGGAC
TMPRSS7	TACGACTCCCTTTTGCCCATCC	GGATTCCTGAGAGCCTCCGTAT
CHRNA9	CTAATGCTCTTCGTCCAGTGGAA	GTGAGATAGGCATCGTGCCAGA
SAA1	TCGTTCCTTGGCGAGGCTTTTG	AGGTCCCCTTTTGGCAGCATCA
EDNRB	CAGAAAGCCTCCGTGGGAATCA	ACAGCCAGAACCACAGAGACCA
ANGPTL3	CCTGAAACTCCAGAACACCCAG	TTCCACGGTCTGGAGAAGGTCT
TNNI3	CTAGTGGCTTGTGATCCCAGCA	GCTTCAGGAGTGTGACAATGGC
MCHR1	AACGCCAGCAACACCTCTGATG	AGATGACCGTGGAGTTCCCGAT
TNFSF11	GCCTTTCAAGGAGCTGTGCAAAA	GAGCAAAAGGCTGAGCTTCAAGC
ABCB6	GTTCTTCAACGCCTGGTTTGGC	AGCACGACGAAACTTGGTTCTCC
CYP27B1	CTCCACTCAGAGATCACAGCTG	GGACACGAGAATTTCCAGGTACC
CCL7	ACAGAAGGACCACCAGTAGCCA	GGTGCTTCATAAAGTCCTGGACC
ATP1A3	GCAACGAGACTGTGGAGGACAT	CGATTTGCTCGGAGGTGAAGTC
JPH4	ATGATGCTGGGTGCCTGACAGA	AGGAAGTAGCCTCAGGTGAGGA
PDK4	AGGTGGAGCATTTCTCGCGCTA	GAATGTTGGCGAGTCTCACAGG
P16	CTCGTGCTGATGCTACTGAGGA	GGTCGGCGCAGTTGGGCTCC
P21	AGGTGGACCTGGAGACTCTCAG	TCCTCTTGGAGAAGATCAGCCG
BAX	TCAGGATGCGTCCACCAAGAAG	TGTGTCCACGGCGGCAATCATC
CDH1	GCCTCCTGAAAAGAGAGTGGAAG	TGGCAGTGTCTCTCCAAATCCG
CDH2	CCTCCAGAGTTTACTGCCATGAC	GTAGGATCTCCGCCACTGATTC
VIM	AGGCAAAGCAGGAGTCCACTGA	ATCTGGCGTTCCAGGGACTCAT
GAPDH	GTCTCCTCTGACTTCAACAGCG	ACCACCCTGTTGCTGTAGCCAA

ensure the precision and reliability of the predictions, a significance threshold of $P \leq 0.05$ was used as the filtering criterion [15].

2.7. Cell culture and transient transfection

The HKb-20 renal epithelial cell line and two KIRC cell lines (786-0 and ACHN) were procured from Beijing Bena Biotechnology Co. (Beijing, China). These cells were maintained in DEME F-12 medium. Lipofectamine 2000 (Invitrogen, Thermo Fisher, USA) was used to transfect the negative control (NC) and ENDRB siRNA (Sagon, China) into the cells(Table 1).

2.8. Quantitative real-time Polymerase Chain reaction (qRT-PCR)

Initially, cells were treated with 1 mL of Trizol (#T9424, Merck, USA) and incubated for 5 min for lysis. Subsequent to cell lysis, the total RNA was extracted and quantified using a NanoDrop 2000 spectrophotometer. The isolated RNA was then transcribed into cDNA (1 μg) and subjected to real-time quantitative PCR analysis. The PCR reaction mixture (20 μL) consisted of 10 μmol of the forward primer, 10 μmol of the reverse primer, UltraSYBR Mixture, 40 ng of cDNA template, and ddH2O. The detection of PCR products was performed using the Light Cycler 96 Real-Time PCR System, with GAPDH utilized as the internal control. Provided below are the sequences of primer pairs for the genes under investigation (Table 2).

2.9. Cell viability

The viability of cells was evaluated using the Cell Counting Kit-8 assay (Beyotime, China), adhering to the guidelines provided by the manufacturer. Different cell treatments were cultured in 96-well plates, with each well containing $1 \times 10^{\wedge 3}$ cells. The CCK-8 reagent was added at designated time points. After a 2-h incubation period at 37 °C, the optical density at 450 nm in each well was recorded with a microplate reader (BioTeK, USA).

2.10. Statistical analyses

The data in this study were presented as mean ± standard error (SD), and group differences were compared using a Student's t-test. Statistical analysis was performed using R version 4.0.2, with a significance level set at $p < 0.05$ (two-tailed) to determine statistical significance.

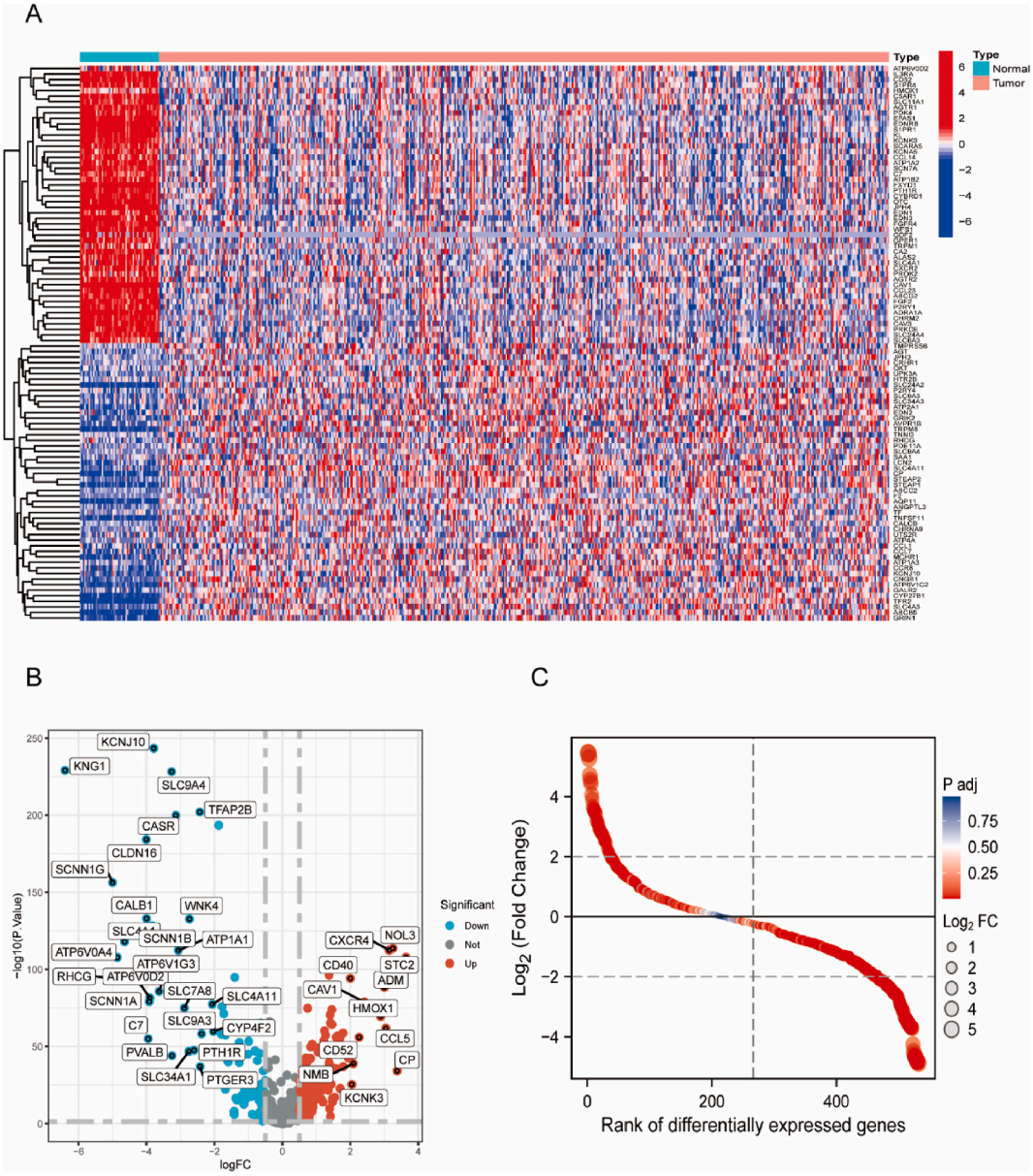

Fig. 1. Screening of differentially expressed Ion Homeostasis-related genes. (A) Heat map showing the variance in expression levels of Ion Homeostasis-related genes in normal and tumor tissues; (B) The volcano plot displays the significance level and fold changes of differentially expressed genes; (C) The sorting chart displays the fold changes and distribution patterns of ion homeostasis related gene expression levels in TCGA-KIRC.

3. Results

3.1. Identification of prognosis-related ion homeostasis genes

The collection of genes related to maintaining "ion balance" was acquired from the Harmony portal, encompassing a total of 524 genes linked with ion homeostasis. Additionally, the "Limma" R package pinpointed 70 ion homeostasis genes with altered expression levels in the TCGA-KIRC group when $|\log FC| > 2$ and $p < 0.05$. The heatmap illustrates the contrast in gene expression levels related to ion homeostasis in normal and tumor tissues within the TCGA-KIRC dataset (Fig. 1A). Meanwhile, the volcano plot shows the fold changes of differentially expressed genes (Fig. 1B), while the ranking plot further clarifies the expression distribution of these genes (Fig. 1C) These results provide a foundation for the construction of subsequent models.

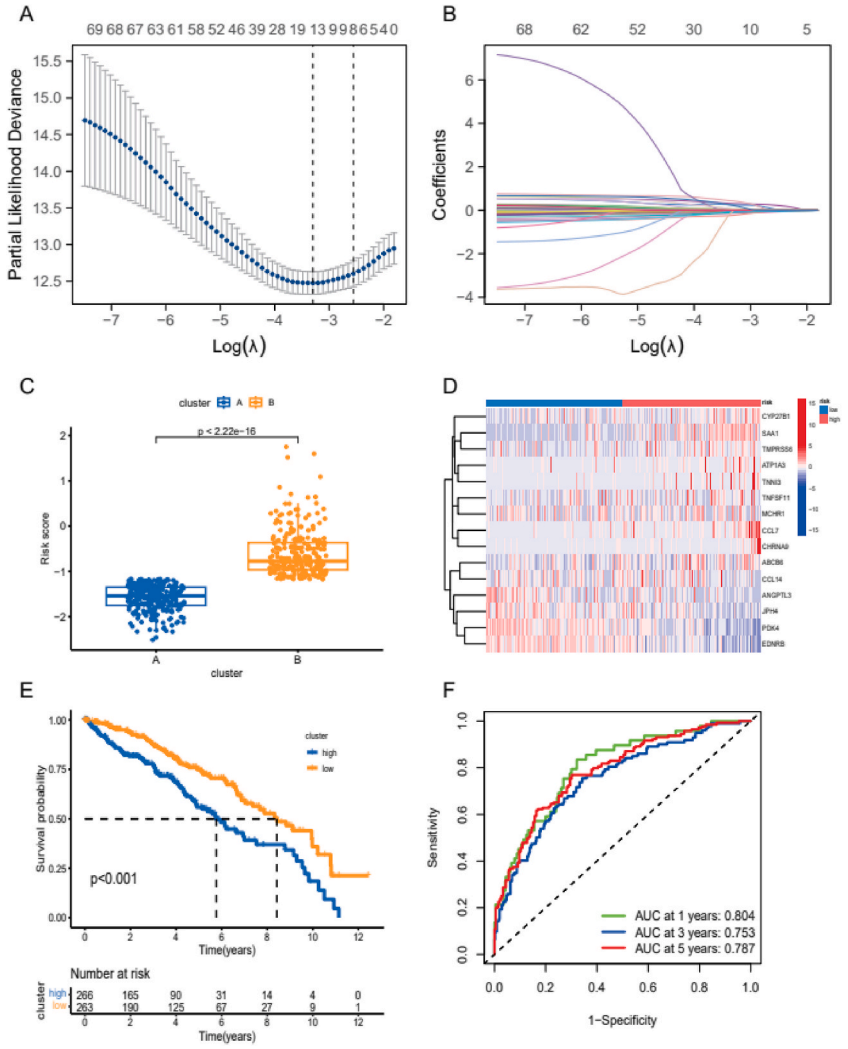

Fig. 2. Development of a prognostic risk score model. (A) LASSO regression analysis shows the coefficient distribution and feature selection process of 70 differentially expressed ion homeostasis related genes; (B) The optimal lambda value determined by LASSO algorithm is used to construct a prognostic risk scoring model; (C) A boxplot depicting the differences in risk coefficients between groups classified as high-risk and low-risk; (D) A heatmap representing notable changes in gene expression associated with prognostic risk; (E) Differences in overall survival prognosis among high-risk and low-risk groups; (F) An ROC curve illustrating the 1-year, 3-year, and 5-year risk scores for overall survival in KIRC patients.

3.2. Construction of lasso model based on ion homeostasis of overall survival in KIRC

Due to the importance of ion balance in the development of tumors, we created a model to diagnose and predict overall survival (OS) in KIRC based on 70 specific genes. This model can be utilized for both diagnostic and predictive regression assessments. Initially, we applied lasso regression analysis to identify the best lambda value and determine 15 genes that are statistically significant. We then constructed a diagnostic model consisting of 15 genes, including PDK4, JPH4, ATP1A3, CCL7, CYP27B1, ABCB6, TNFSF11, MCHR1, TNNI3, ANGPTL3, EDNRB, SAA1, CHRNA9, TMPRSS6, and CCL14. Utilizing the LASSO Logit model algorithm enabled the attainment of lambda and Min values visualization, while stability was maintained by establishing a loss function for LASSO (Fig. 2A–B). The risk scoring model divides patients into high-risk and low-risk groups, the statistically significant difference between the high-risk and low-risk groups was confirmed by heat maps and box plots (Fig. 2C–D). Kaplan Meier survival analysis further showed that the overall survival of high-risk group patients was significantly lower than that of low-risk group patients (Fig. 2E). Additionally, ROC curve analysis validated the significant value of the risk scoring model in predicting patient prognosis, with AUC values of 1 year (0.804), 3 years (0.753), and 5 years (0.787), indicating that the model has high predictive power (Fig. 2F). Furthermore, we validated the prognostic model in the E-MTAB-1980 dataset. The results of the validation set are consistent with those of the training set. The overall survival outcomes of the low-risk group are significantly better (Supplementary Fig. 1A). The AUC values for the one-year, three-year, and five-year ROC curves of the risk score are 0.768, 0.755, and 0.766, respectively (Supplementary Fig. 1B). This further confirms that

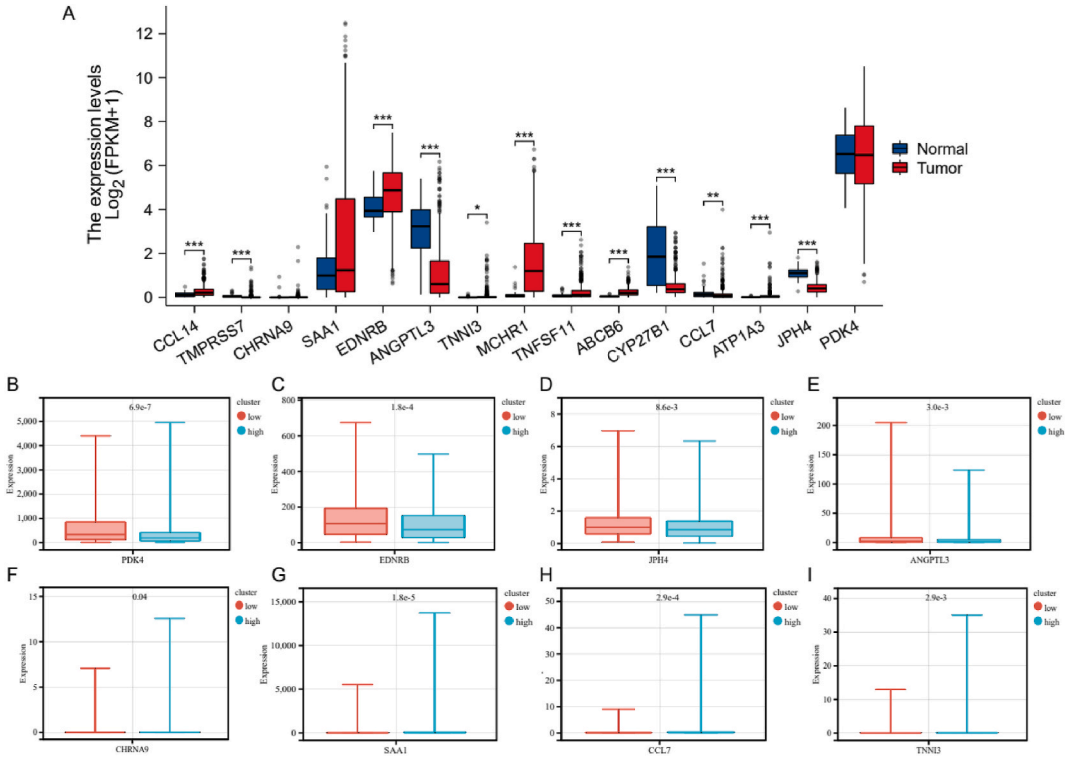

Fig. 3. Expression differences of prognostic risk genes associated with Ion Homeostasis. (A) Variances in the expression levels of prognostic risk genes in normal versus tumor tissues; (B–I) Visualization of expression levels of prognostic risk genes showcasing notable distinctions among various risk categories.

the risk gene model has significant prognostic significance. These results indicate that our model can effectively distinguish the survival risk levels of KIRC patients.

The difference in expression levels of CCL14, TMPRSS7, SAA1, EDNRB, ANGPTL3, TNNI3, MCHR1, TNFSF11, ABCB6, CYP27B1, CCL7, ATP1A3, JPH4, and PDK4 was then calculated in the risk model (Fig. 3A). Notable variances were noted in the levels of expression for EDNRB, PDK4, ATP1A3, JPH4, CHRNA9, CCL7, SAA1, and TNNI3 between the groups with high and low risks (see Fig. 3B–I). These genes may play important roles in the tumor biology and immune microenvironment regulation of KIRC.

3.3. Establishment and validation of a prognostic nomogram for KIRC

The nomogram acts as an efficient instrument for predicting both immediate and extended survival probabilities in KIRC patients. By considering clinicopathologic factors, we combined the risk model score with clinical information to create an all-encompassing nomogram (Fig. 4A). The calibration graph validates the nomogram's accuracy (Fig. 4B). Furthermore, cumulative risk graphs demonstrated a steady rise in overall survival risk for patients with higher KIRC scores as shown in the nomogram (Fig. 4C). Decision curve analysis (DCA), applicable at intervals of 1, 3, and 5 years, is a simple technique frequently utilized in clinical settings to assess predictive models, diagnostic measures, and molecular indicators to establish the efficacy of a strategy for patient benefit (Fig. 4D–F). These findings imply that the prognostic nomogram, built upon the Ion Homeostasis risk score, can be utilized as an efficient clinical tool for predicting patient outcomes.

3.4. Gene enrichment analysis

In order to better understand the biological importance of six stem cell-related marker models in KIRC, extensive functional enrichment studies were carried out on genes of various sizes and levels using GO enrichment analysis. By utilizing the KEGG database, which includes comprehensive information on genomes, biological pathways, diseases, and medications, all markedly differentially expressed genes underwent GO function annotation through R-package clustering tools to identify significantly enriched biological processes. The results of the enrichment were visually represented using the R package GO plot. Additionally, the R package clusterprofiler was utilized to annotate all markedly differentially expressed genes with GO function, aiding in the identification of significantly enriched biological processes. The resulting enrichment analyses highlighted the predominance of cellular components such as the apical plasma membrane, apical cell region, caveola, transmembrane transporter complex, and transporter complex in genes associated with ion homeostasis prognosis. In terms of biological functions, the primary focus was on maintaining calcium ion

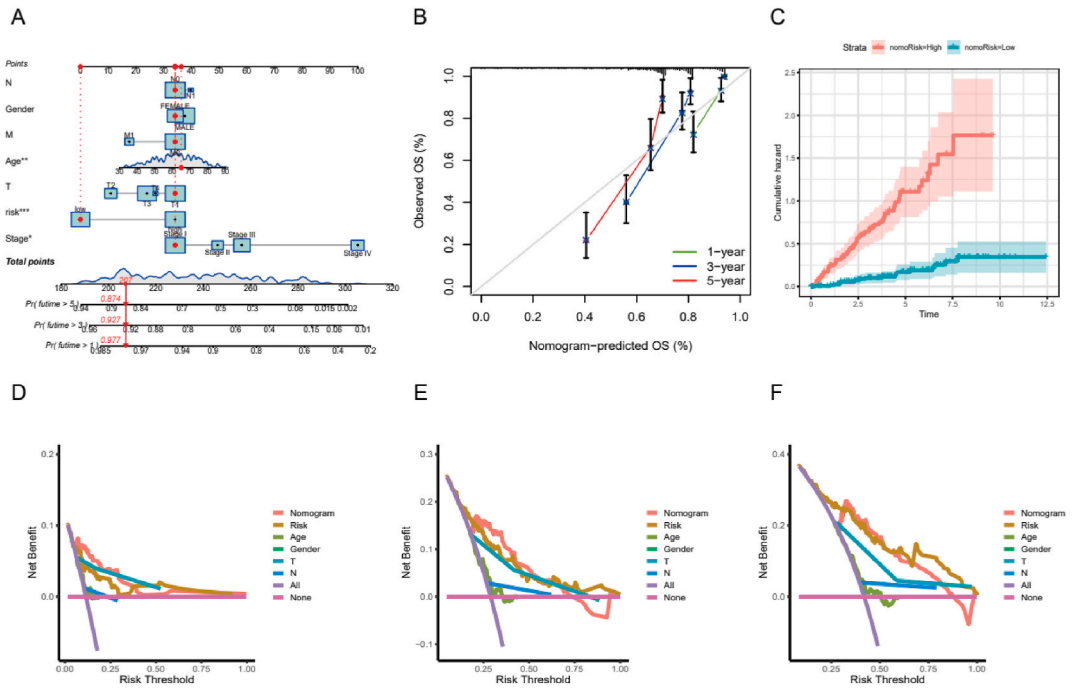

Fig. 4. Validation of diagnostic models. (A) A nomogram constructed from the ion homeostasis-related prognostic signature; (B) Internal validation calibration curves for the nomogram; (C) The cumulative event plot shows an increasing trend in the overall survival risk of KIRC patients with higher scores; (D–F) Decision Curve Analysis (DCA) evaluates the clinical utility of column charts in predicting 1-year, 3-year, and 5-year survival, demonstrating their significant advantages at different time intervals. $^{**}p < 0.01$, $^{***}p < 0.001$.

levels within cells, balancing cellular calcium ion concentrations, managing divalent inorganic cations within cells, controlling the concentration of calcium ions in the cytosol, and promoting an increase in cytosolic calcium ions. Molecular activities of interest included the movement of potassium ions across cell membranes, transporting metal ions across cell membranes, binding to G protein-coupled receptors, binding to hormones, and interacting as a ligand with receptors (Fig. 5A,B,D,G). The forecasting model was associated with pathways such as interactions between neuroactive ligands and receptors, signaling through cyclic AMP, the absorption of minerals, signaling in cardiomyocytes via adrenergic pathways, and the secretion of gastric acid (Fig. 5C,E,F,H).

3.5. Gene set enrichment analysis of prognostic risk model

To better understand the role of ion homeostasis-related genes in KIRC, we based on the expression of 15 prognostic DEGs, the GSVA package was applied to identify more significant differential enrichment of phenotypic gene sets and KEGG pathways between high and low risk. It is suggested that cluster B, which has the worst prognosis in the high-risk group, is mainly enriched in amino acid- and bile-related metabolic processes, ion transport, cytoplasmic transporter membrane adapters, transporter activity, and so on (Supplementary Fig. 2A). At the same time, they were enriched in lysine degradation, vasopressin regulation, APLN signaling pathway, renin Angiotensinogen system, tricarboxylic acid cycle, TCA cycle metabolism, etc. (Supplementary Fig. 2B)

3.6. Gene expression and immune infiltration in three subtype clusters

The immune microenvironment is a critical factor in the process of tumorigenesis, progression, and reaction to immunotherapy. To enhance our comprehension, we conducted a thorough investigation into the TME in individuals at both high and low risk for KIRC. Employing the CIBERSORT r script, we quantified the infiltration of immune cells in these individuals. Through the classification of samples according to their risk assessment, we could analyze the relationship between the distribution of diverse immune cells and the degree of risk in each patient (Fig. 6A). Moreover, low-risk KIRC patients displayed a significant increase in both resting memory CD4 T cells and activated memory CD4 T cells; In contrast, high-risk KIRC patients with unfavorable prognoses exhibited a higher percentage of follicular helper T cells and regulatory T cells (Tregs) (Fig. 6B). This relationship is linked to the potential for immune cell infiltration to serve as a prognostic indicator. Analyzing the correlations between immune cell types in KIRC patients can offer valuable insights into the immune microenvironment dynamics over time (Fig. 6C). The risk model developed using the 15-gene signatures revealed unique expression patterns in both high-risk and low-risk groups, and these patterns were strongly associated with different immune cell infiltrations (Fig. 6D). The presence of follicular helper T cells, regulatory T cells (Tregs), and activated memory CD4 T cells increased progressively with the rise in risk scores (Fig. 7A–C). On the other hand, the proportions of resting mast cells, monocytes,

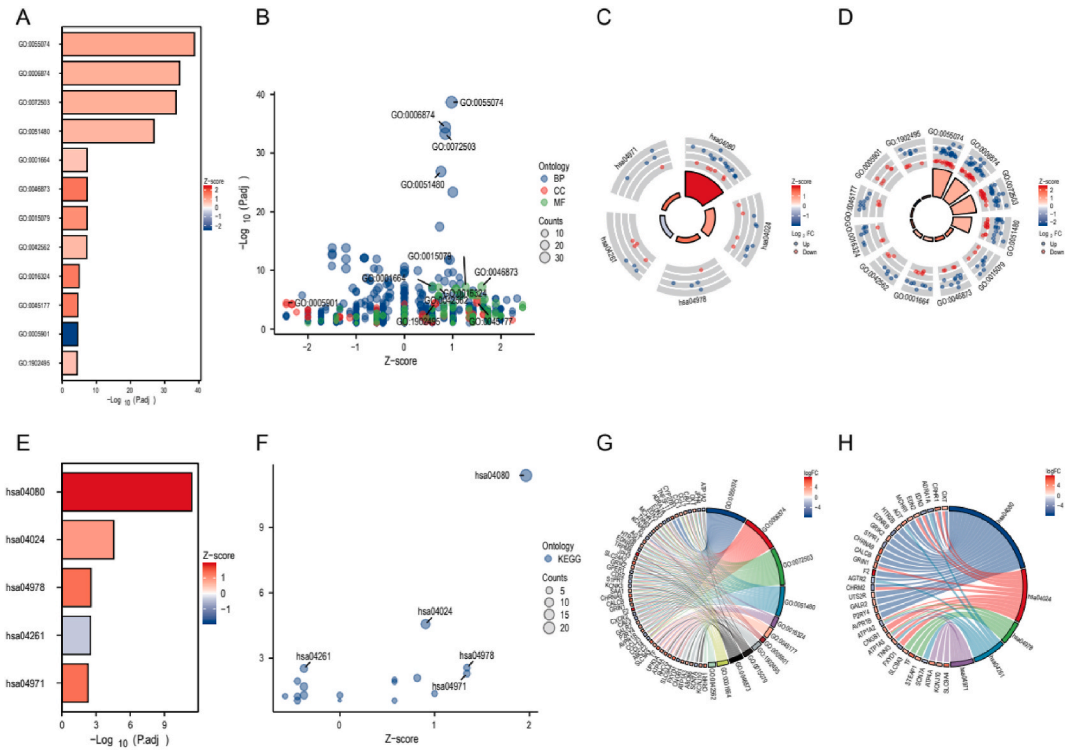

Fig. 5. Enrichment analysis of ion homeostasis-related prognostic genes. (A–B) Bar plot and bubble plot displaying results of GO enrichment analysis; (C) Bubble plot for GO enrichment analysis; (D) Bubble plot illustrating KEGG enrichment analysis. (E–F) Bar plot and bubble plot showcasing the outcomes of KEGG enrichment analysis; (G–H) Enrichment Network diagram for both GO and KEGG analyses.

resting memory CD4 T cells, M1 macrophages, and M2 macrophages decreased as the risk scores rose (Fig. 7D–H). These findings indicate that our prognostic model, which incorporates key differentially expressed genes related to ion homeostasis, is strongly connected to the tumor immune microenvironment of KIRC.

3.7. Experimental verification of cell biology

We first detected markers predicted by bioinformatics by QPCR. We found a significant elevation in EDNRB in KIRC cell lines 786-0 and ACHN compared to HKb-20 in human renal epithelial cells (Fig. 8A–C). We selected EDNRB for subsequent experiments. Two small interfering RNAs for different targets significantly inhibited EDNRB expression in 786-0 and ACHN cell lines (Fig. 8D). Cell viability of 786-0 and ACHN was significantly inhibited after interfering with EDNRB expression (Fig. 8E).

After interfering with EDNRB expression, the transcript levels of cellular senescence markers, P16 and P21, were significantly upregulated. The upregulation of P16 and P21 was accompanied by the upregulation of BAX, an indicator of apoptosis (Fig. 9A–B). Finally, we also examined cellular EMT markers after interference with EDNRB expression, after which CDH1 expression was restored and CDH2 and VIM expression was suppressed (Fig. 9C–D). These results further confirm the crucial role of EDNRB in KIRC cell proliferation, apoptosis, and invasion.

4. Discussion

Renal clear cell carcinoma of the kidney is a prevalent subtype of renal cell carcinoma, displaying significant diversity in metastatic potential and immunoreactivity [16]. Due to the rapid advancement of the illness, enhancing patient prognosis via a singular targeted pathway or medication regimen proves challenging [17]. Ion channels are highly expressed in both excitable and non-excitable cells. A unique function of the immune system is its involvement in identifying and eradicating tumor cells, which is governed by a variety of ion channels. Tumor cells exhibit a greater level of polarization in their ion channels compared to immune cells, impacting both tumor cell growth and spread. Consequently, targeting ion channels is crucial in the development of therapies for combating tumors. Consequently, the development of prognostic models utilizing genes associated with ion homeostasis could serve as a valuable resource for preemptive measures [18]. Nonetheless, the current inventory of such markers remains insufficient [19]. Hence, an immediate demand exists for the identification of additional biomarkers possessing elevated predictive efficacy to supplement the roster of potential candidates.

Nevertheless, the quantity of these markers falls short. It is imperative to assess additional biomarkers that exhibit superior

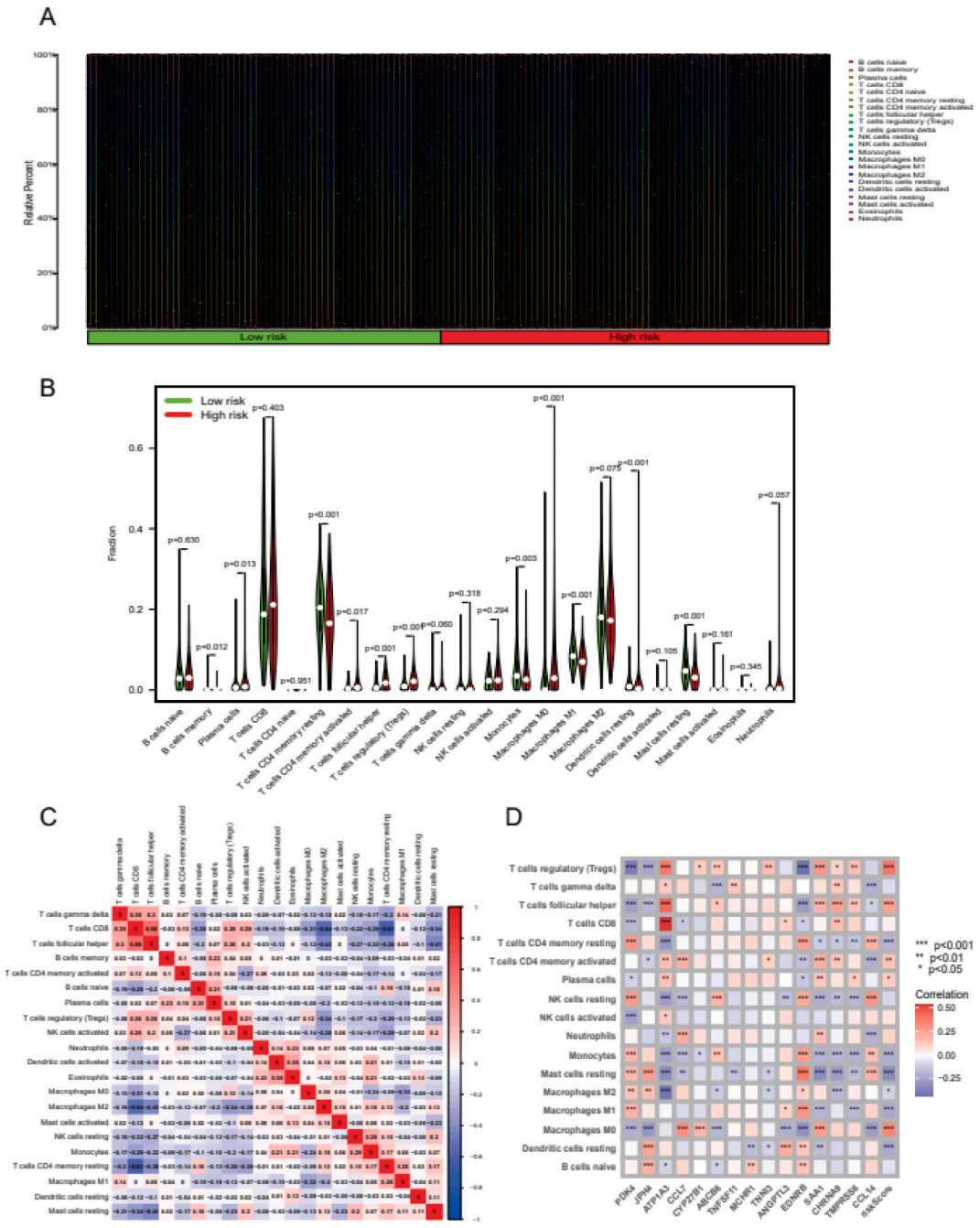

Fig. 6. Evaluation of immune infiltration. (A) Bar charts representing the distribution of immune cells infiltrating both high-risk and low-risk categories; (B) Boxplots highlighting the differences in immune cell infiltration levels between high-risk and low-risk categories; (C) A heatmap illustrating the correlation among the distributions of infiltrating immune cells; (D) A heatmap depicting the relationship between markers associated with ion homeostasis and immune cell infiltration levels. * <0.05; *** <0.001.

predictive capabilities for potential incorporation in prospect lists. Therefore, we constructed an ion homeostasis-related prognostic model by analyzing a total of 537 tumor samples containing clinical data and 72 paratumor tissues from the TCGA-KIRC cohort, potentially providing an important tool for early intervention.

In this study, we identified 15 risk genes (PDK4, JPH4, ATP1A3, CCL7, CYP27B1, ABCB6, TNFSF11, MCHR1, TNNI3, ANGPTL3, EDNRB, SAA1, CHRNA9, TMPRSS6, CCL14). Earlier investigations have outlined specific connections between genes and the initiation and progression of cancer [20]. CC chemokines, a subfamily of 27 chemokines, are important components of cell-to-cell communication and are essential for the function of the tumor microenvironment [21,22]. Pyruvate dehydrogenase kinase 4(PDK4) has been

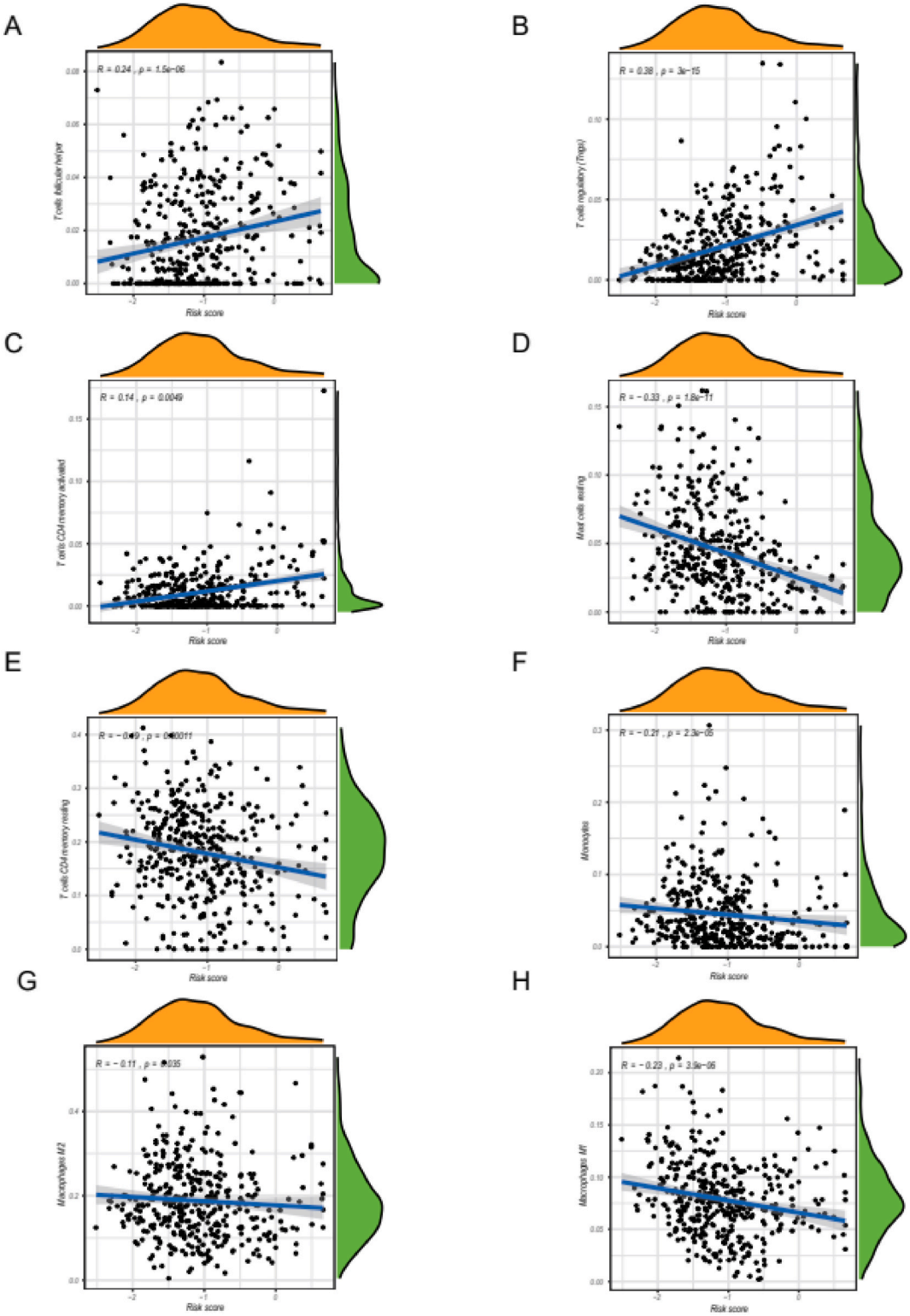

Fig. 7. Correlation of prognostic risk with immune cell infiltration. (A–C) A scatter plot showing a positive correlation between the risk score of the prognostic model and the level of immune cell infiltration; (D–H) A scatter plot illustrating a negative correlation between the risk score of the prognostic model and the extent of immune cell infiltration.

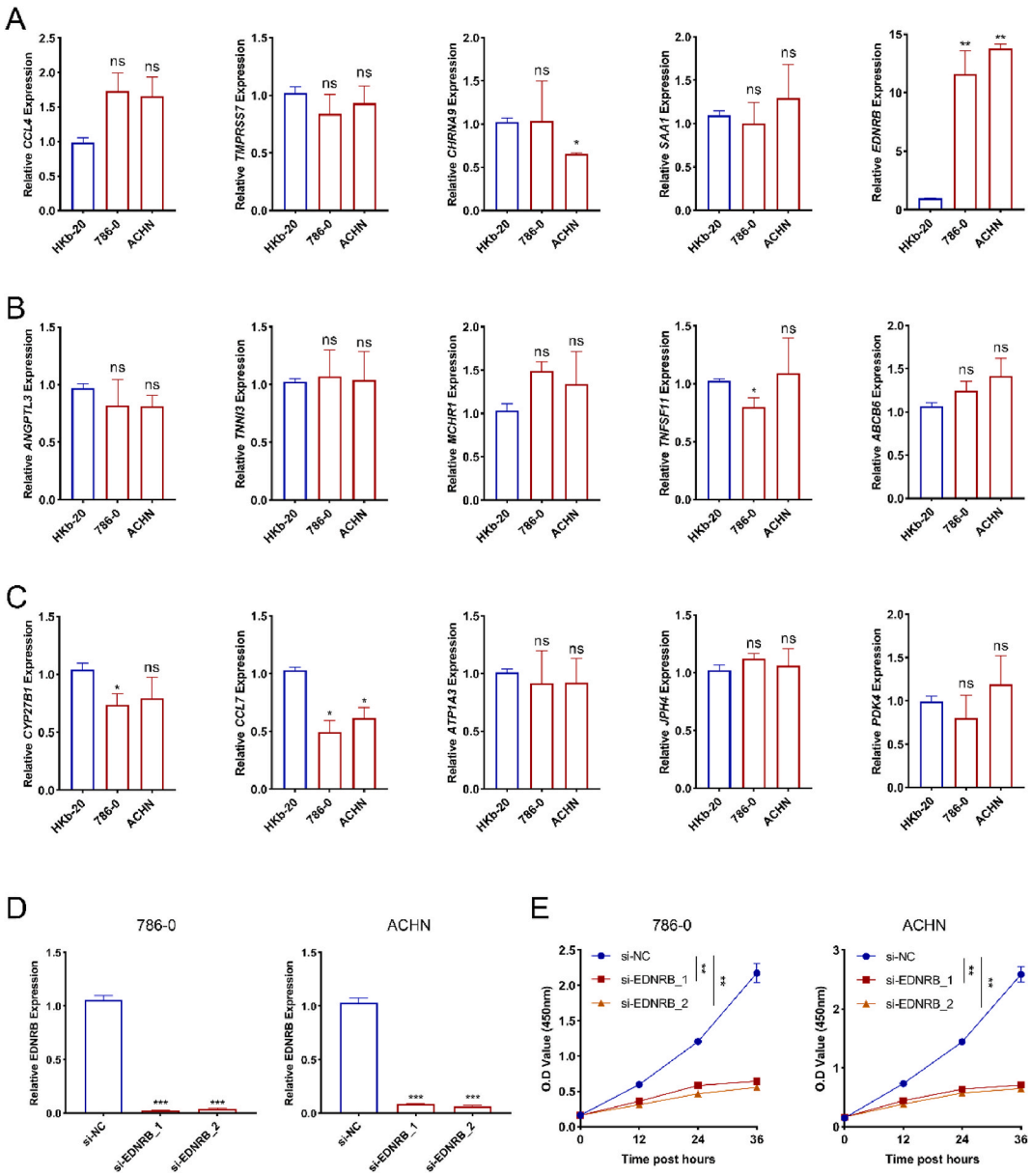

Fig. 8. *EDNRB* was significantly upregulated in KIRC cell lines. (A–C) PCR detection of molecular markers mined by bioinformatics. (D) The efficiency of small interfering RNAs to inhibit *EDNRB* expression was tested in 786-0 and ACHN cell lines. (E) Cell viability of 786-0 and ACHN cell lines was examined after interfering with *EDNRB* expression. N = 3/group. *≤0.05, **≤0.01.

used as a biomarker of energy metabolism pathways, and in vitro experiments and single-cell sequencing analysis have suggested that it is associated with energy metabolism in proximal tubular cells [23]. ABCB6 of the ATP-binding cassette transporter family (ABC) transporter family can transport various molecules through extracellular and intracellular membranes, and its overexpression confers tolerance to cadmium and AS2O3 [24]. Overexpression of ABCB6 enhanced resistance to the antitumor drugs SN-38 and vincristine, suggesting that the transporter is a potential anticancer therapeutic target [25,26]. In addition, the genes of EDNRB, CHRNA9, SAA1, TNNI3, Ednrb and MCHR1 in the prognostic model were related to the migration/invasion ability of cells and some regulatory functions of tumor respectively [13,27–29]. [30].

Based on the pre-defined Gene expression profiling of LASSO model, 15 genetic markers were screened to effectively identify patients' prognosis. Clinicians can develop more individualized treatment strategies by utilizing nomograms based on 15 gene features for patients with KIRC at different time points. By examining the effect of prognostic risk models on immune cell infiltration in KIRC, researchers can deepen their understanding of the microenvironment interactions. Further analysis shows a significant correlation between the model and immune cell infiltration characteristics, providing a new perspective for a deeper understanding of the complex

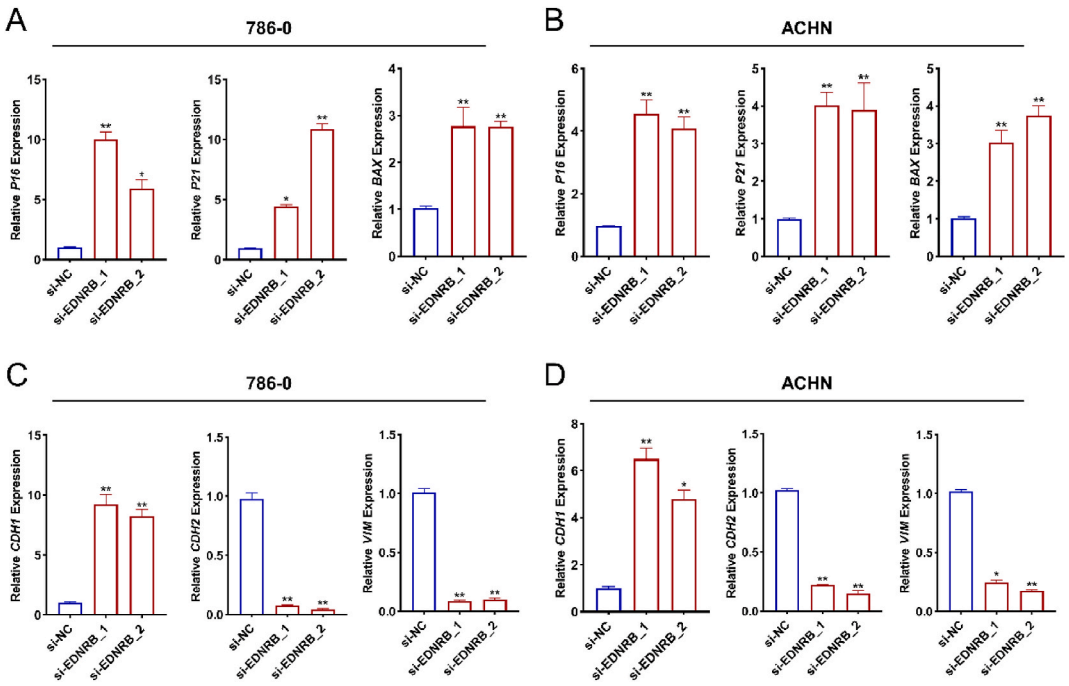

Fig. 9. *EDNRB inhibition promotes cellular senescence, apoptosis and inhibits EMT in renal clear cell carcinoma.* (A–B) EDNRB inhibition promotes senescence, apoptosis in cell lines 786-0 and ACHN of renal clear cell carcinoma. (C–D) EDNRB inhibition suppressed EMT in cell lines 786-0 and ACHN of renal clear cell carcinoma. N = 3/group. *≤0.05, **≤0.01.

interaction between tumor microenvironment and immune response. In our study, high-risk patients with poor prognosis were significantly positively correlated with Tregs. Tregs can secrete immunosuppressive cytokines, leading to T cell dysfunction [31,32]. Previous studies have shown that Treg can inhibit the protective function of CD8+T cells in KIRC and prevent tumor cells from immune attacks [33]. Elevated Treg infiltration in KIRC can lead to clinical treatment failure and is associated with poor prognosis in KIRC patients [34–36]. In recent years, the key role of ion channels in immune cell differentiation, maintenance, and activation has received widespread attention. Ionic channels play an important role in immune regulation by regulating membrane potential, calcium signaling pathways, and immune cell effector functions [37,38]. Especially in Tregs, the regulation of ion homeostasis and its impact on immune suppression function have gradually become a research hotspot [39]. TRPM7 is an ion channel capable of transporting cations such as Ca2+、Na+、Zn2+, and Mg2+, and is highly expressed in T cells [40]. Mendu et al. found that blocking TRPM7 channel activity increases the development of IL-2-dependent thymic Tregs (tTreg). The activity of TRPM7 can increase the number of Tregs in the body and promote immune tolerance, indicating its value as a potential therapeutic target [41]. However, the specific mechanism of action of Tregs and ion channels in KIRC is still not fully understood, which provides new directions and possibilities for future research and treatment strategies.

Although the prognostic model constructed in this study showed good predictive performance in KIRC patients, there are still some limitations. Firstly, the model is based on TCGA-KIRC queue data. Future research should validate the stability and applicability of the model on larger scale multi center datasets. In addition, although this study has preliminarily explored the potential biological mechanisms of genes, further validation of the specific functions and mechanisms of these genes in renal clear cell carcinoma through in vitro experiments and animal models is still needed. Finally, the study did not fully explore the interactions between genes and their synergistic effects on the tumor microenvironment, which provides important directions for future research.

5. Conclusion

This study constructed an accurate prognostic model by integrating ion homeostasis related genes, revealing the key role of ion channels in renal clear cell carcinoma. This model not only provides an important tool for personalized treatment of patients, but also offers new ideas for in-depth research on the relationship between tumor microenvironment and immune response. In the future, through further validation and functional research, it is expected that these genes will be used as potential therapeutic targets to promote the development of precision medicine in KIRC.

CRediT authorship contribution statement

Xiangmin Zhang: Writing – original draft, Software, Resources, Methodology, Formal analysis, Data curation, Conceptualization.

Xiongxian Qian: Writing – review & editing, Writing – original draft, Software, Resources, Data curation, Conceptualization. **Yong Zhao:** Writing – review & editing, Writing – original draft, Visualization, Methodology, Conceptualization. **Maofei Ye:** Writing – review & editing, Writing – original draft, Software, Formal analysis, Data curation. **Liyang Li:** Writing – original draft, Formal analysis. **Jian Chu:** Writing – review & editing, Writing – original draft, Software, Resources, Data curation, Conceptualization.

Data statement

Data will be made available on request. For requesting data, please write to the corresponding author.

Funding

This work was funded by Baoshan District Health Commission Excellent Youth(Yucai)Program(BSWSYC-2024-16) and Baoshan District Health Commission Key Subject Construction Project(BSZK-2023-A06)

Declaration of competing interest

The authors declare that they have no known competing financial interests or personal relationships that could have appeared to influence the work reported in this paper.

Appendix A. Supplementary data

Supplementary data to this article can be found online at https://doi.org/10.1016/j.heliyon.2025.e41736.

References

[1] J F, M C, I S, et al. - Cancer Incidence and Mortality Patterns in Europe: Estimates for 40 Countries and. *D - 9005373*. (- 1879-0852 (Electronic)):- 356-387.
[2] Y. Liu, M. Grimm, W.T. Dai, M.C. Hou, Z.X. Xiao, Y. Cao, CB-Dock: a web server for cavity detection-guided protein-ligand blind docking, Acta Pharmacol. Sin. 41 (1) (2020) 138–144.
[3] X. Huang, B. Zha, M. Zhang, et al., Decreased monocyte count is associated with gestational diabetes mellitus development, macrosomia, and inflammation, J. Clin. Endocrinol. Metabol. 107 (1) (2022) 192–204.
[4] L. B, K. G, Biological functions of autophagy genes: a disease perspective, Cell 176 (1–2) (2019 Jan 10) 11–42, 101016/jcell201809048. (- 1097-4172 (Electronic)):- 11-42.
[5] Q. Zhang, Y. Kong, Z. Yang, Y. Liu, R. Liu, Y. Geng, H. Luo, H. Zhang, H. Li, S. Feng, X. Wang, Preliminary study on radiosensitivity to carbon ions in human breast cancer, Journal of radiation research 61 (2020) 399–409, https://doi.org/10.1093/jrr/rraa017.
[6] V. Falcone, G. Kotzaeridi, M.H. Breil, et al., Early assessment of the risk for gestational diabetes mellitus: can fasting parameters of glucose metabolism contribute to risk prediction? Diabetes & metabolism journal 43 (6) (2019) 785–793.
[7] Q F, L X, Y W, et al. - Tumor-associated Macrophage-Derived Interleukin-23 Interlinks Kidney Cancer. *D - 7512*719. (- 1873-7560 (Electronic)):- 752-763.
[8] Cm D-M, Bi R, Jh F. - The Immunology of Renal Cell Carcinoma. *D - 101500081*. (- 1759-507X (Electronic)):- 721-735.
[9] R. Me, P. B, W. D, et al., - limma powers differential expression analyses for RNA-sequencing and microarray, Nucleic Acids Res. 43 (7) (2015 Apr 20) e47. *101093/nar/gkv007 Epub 2015 Jan.* (- 1362-4962 (Electronic)):- e47.
[10] Y. Guo, Z. Han, L. Guo, et al., Identification of urinary biomarkers for the prediction of gestational diabetes mellitus in early second trimester of young gravidae based on iTRAQ quantitative proteomics, Endocr. J. 65 (7) (2018) 727–735.
[11] T.L. Barke, J.A. Goldstein, A.C. Sundermann, et al., Gestational diabetes mellitus is associated with increased CD163 expression and iron storage in the placenta, American journal of reproductive immunology (New York, NY : 1989) 80 (4) (2018) e13020.
[12] P. Furió-Tarí, S. Tarazona, T. Gabaldón, A.J. Enright, A. Conesa, spongeScan: a web for detecting microRNA binding elements in lncRNA sequences, Nucleic Acids Res. 44 (W1) (2016) W176–W180.
[13] B.E. Metzger, L.P. Lowe, A.R. Dyer, et al., Hyperglycemia and adverse pregnancy outcomes, N. Engl. J. Med. 358 (19) (2008) 1991–2002.
[14] Pj H, Y Z. - Survival Model Predictive Accuracy and ROC Curves. *D - 0370625*. (- 0006-341X (Print)):- 92-105.
[15] Am N, Cl L, Mr G, et al. - Robust enumeration of cell subsets from tissue expression profiles. D - 101215604. (- 1548–7105 (Electronic)):- 453-457.
[16] C. Billionnet, D. Mitanchez, A. Weill, et al., Gestational diabetes and adverse perinatal outcomes from 716,152 births in France in 2012, Diabetologia 60 (4) (2017) 636–644.
[17] Jh W, Zh F, Y C, et al. - Predictive value of single-nucleotide polymorphism signature for recurrence in. D - 100957246. (- 1474-5488 (Electronic)):- 591-600.
[18] Z. Ma, D. Yuan, X. Cheng, B. Tuo, X. Liu, T. Li, Function of ion transporters in maintaining acid-base homeostasis of the mammary gland and the pathophysiological role in breast cancer, American journal of physiology. Regulatory, integrative and comparative physiology. 318 (2020) R98–r111, https://doi.org/10.1152/ajpregu.00202.2019.
[19] W X, J W, X W, et al. - Therapeutic targeting of the USP2-E2F4 axis inhibits autophagic machinery. D - 101265188. (- 1554-8635 (Electronic)):- 2615-2635.
[20] Z. Wang, Y. Yang, Y. Cui, C. Wang, Z. Lai, Y. Li, W. Zhang, H. Mustonen, P. Puolakkainen, Y. Ye, K. Jiang, Z. Shen, S. Wang, Tumor-associated macrophages regulate gastric cancer cell invasion and metastasis through TGFβ2/NF-κB/Kindlin-2 axis, Chinese journal of cancer research = Chung-kuo yen cheng yen chiu 32 (2020) 72–88, https://doi.org/10.21147/j.issn.1000-9604.2020.01.09.
[21] H W, X Z, D H, J C, J T. - Tumour-associated macrophages mediate the invasion and metastasis of bladder. D - 101603425. (- 2167-8359 (Print)):- e8721.
[22] D H, Ra W. - Hallmarks of Cancer: the Next Generation. *D - 0413*066. (- 1097-4172 (Electronic)):- 646-674.
[23] X S, J L, F K, et al. - PDK4 Dictates Metabolic Resistance to Ferroptosis by Suppressing Pyruvate. D – 101573691. (- 2211-1247 (Electronic)):- 108767.
[24] C W, Id O, C C, et al. - Cryo-electron Microscopy Structure of Human ABCB6 Transporter. *D - 9211*750. (- 1469-896X (Electronic)):- 2363-2374.
[25] V. Helias, C. Saison, B.A. Ballif, T. Peyrard, J. Takahashi, H. Takahashi, M. Tanaka, J.C. Deybach, H. Puy, M. Le Gall, C. Sureau, B.N. Pham, P.Y. Le Pennec, Y. Tani, J.P. Cartron, L. Arnaud, ABCB6 is dispensable for erythropoiesis and specifies the new blood group system Langereis, Nature genetics 44 (2012) 170–173, https://doi.org/10.1038/ng.1069.
[26] K M, Y K, Y N, et al. - Expression of ABCB6 Is Related to Resistance to 5-FU, SN-38 and Vincristine. *D - 8102*988. (- 1791-7530 (Electronic)):- 4767-4773.
[27] P. Antra, H. Parashar, A. Hungyo, S. Jain, V. Ahmad, Tandon, Unraveling molecular mechanisms of head and neck cancer, Critical reviews in oncology/hematology. 178 (2022) 103778. https://doi.org/10.1016/j.critrevonc.2022.103778.

[28] Nn P, Cy W, Yc L. - The Novel Regulations of MEF2A, CAMKK2, CALM3, and TNNI3 in Ventricular. D - 0361055. (- 1879-3185 (Electronic)):- 123-135.
[29] A.E. Louiselle, S.M. Niemiec, C. Zgheib, K.W. Liechty, Macrophage polarization and diabetic wound healing, Transl. Res. : J. Lab. Clin. Med. 236 (2021) 109–116.
[30] C. Li, M.M. Xu, K. Wang, A.J. Adler, A.T. Vella, B. Zhou, Macrophage polarization and meta-inflammation, Transl. Res. : J. Lab. Clin. Med. 191 (2018) 29–44.
[31] D.E. Speiser, P.C. Ho, G. Verdeil, Regulatory circuits of T cell function in cancer, Nat. Rev. Immunol. 16 (10) (2016) 599–611.
[32] E.J. Wherry, M. Kurachi, Molecular and cellular insights into T cell exhaustion, Nat. Rev. Immunol. 15 (8) (2015) 486–499.
[33] F.C. Thistlethwaite, E. Elkord, R.W. Griffiths, et al., Adoptive transfer of T(reg) depleted autologous T cells in advanced renal cell carcinoma, Cancer immunology, immunotherapy : CII. 57 (5) (2008) 623–634.
[34] M. Sharma, H. Khong, F. Fa'ak, et al., Bempegaldesleukin selectively depletes intratumoral Tregs and potentiates T cell-mediated cancer therapy, Nat. Commun. 11 (1) (2020) 661.
[35] X.D. Liu, A. Hoang, L. Zhou, et al., Resistance to antiangiogenic therapy is associated with an immunosuppressive tumor microenvironment in metastatic renal cell carcinoma, Cancer Immunol. Res. 3 (9) (2015) 1017–1029.
[36] B. Shang, Y. Liu, S.J. Jiang, Y. Liu, Prognostic value of tumor-infiltrating FoxP3+ regulatory T cells in cancers: a systematic review and meta-analysis, Sci. Rep. 5 (2015) 15179.
[37] M.D. Cahalan, K.G. Chandy, The functional network of ion channels in T lymphocytes, Immunol. Rev. 231 (1) (2009) 59–87.
[38] P. Ehling, S. Bittner, T. Budde, H. Wiendl, S.G. Meuth, Ion channels in autoimmune neurodegeneration, FEBS Lett. 585 (23) (2011) 3836–3842.
[39] L. Vinnenberg, S. Bock, P. Hundehege, T. Ruck, S.G. Meuth, Impact of diverse ion channels on regulatory T cell functions, Cell. Physiol. Biochem. : international journal of experimental cellular physiology, biochemistry, and pharmacology 55 (S3) (2021) 145–156.
[40] J. Jin, B.N. Desai, B. Navarro, A. Donovan, N.C. Andrews, D.E. Clapham, Deletion of Trpm7 disrupts embryonic development and thymopoiesis without altering Mg2+ homeostasis, Science (New York, NY) 322 (5902) (2008) 756–760.
[41] S.K. Mendu, M.E. Stremska, M.S. Schappe, et al., Targeting the ion channel TRPM7 promotes the thymic development of regulatory T cells by promoting IL-2 signaling, Sci. Signal. 13 (661) (2020).